ภาคผนวก

Journal of Ceramic Processing Research. Vol. 11, No. 4, pp. 419~424 (2010)

J O U R N A L O F
Ceramic Processing Research

Enhancement of optical bandgap and luminescent characteristics of one-dimensional ZnO nanoparticles

Sumetha Suwanboon[a,*], Pongston Amornpitoksuk[b] and Supasarote Muensit[c]

[a]*Materials Science Program, Faculty of Science, Prince of Songkla University, Hat Yai, Songkhla, 90112, Thailand*

[b]*Department of Chemistry and Center for Innovation in Chemistry, Faculty of Science, Prince of Songkla University, Hat Yai, Songkhla, 90112, Thailand*

[c]*Department of Physics, Faculty of Science, Prince of Songkla University, Hat Yai, Songkhla, 90112, Thailand*

One-dimensional ZnO nanoparticles were successfully synthesized from $Zn(CH_3COO)_2.2H_2O$ as well as CTAB-assisted NaOH and CTAB-assisted HMTA solutions. The entire calcined ZnO nanoparticles indexed with the hexagonal or wurtzite structure. Branch rod-like and columnar hexagonal-like ZnO structures were shaped when aqueous NaOH and HMTA solutions were used as the precipitating agent, respectively. In this study, the crystallite size decreased as the CTAB concentration was increased. By using an aqueous NaOH solution as the precipitating agent, the E_g value varied in a range of 3.222-3.235 eV. While the E_g value varied in a range of 3.206-3.216 eV when an aqueous HMTA solution was used. The emission peaks fitted with a Gaussian function at 390, 510, 620 and 730 nm and the defects in ZnO crystal were decreased by modifying the precursor solution with CTAB.

Key words: Nanostructured materials, Zinc oxide, Precipitation, Optical properties, X-ray diffraction.

Introduction

In the past few years, research and development effort in controlling the shape and size of ZnO particles have been extensively investigated due to their numerous applications. As we know, ZnO is a semiconducting compound that has been used increasingly in various fields due to its outstanding physical and chemical properties. ZnO is an n-type II-VI semiconductor with a wide band gap energy of 3.3 eV and large exciton binding energy of about 60 meV at room temperature which provides a great potential in applications such as gas sensors [1], surface acoustic devices [2], as a rubber additive [3] in solar cells [1] and as a photocatalyst with high chemical activity [4]. It is well-known that the optical properties of ZnO depend closely on its structural properties such as crystallite size, orientation, aspect ratio and particle shape. Therefore, morphological control is a challenge to prepare different ZnO shapes with few agglomerations and a narrow size distribution. Recently, the utilization of a capping agent to control the morphology of ZnO is an interesting route for reducing the size and also providing monosized particles. To date, a number of capping agents have been investigated, for example, polyvinylpyrrolidone (PVP) [5], triethanolamine (TEA) [6], polyol [7] and cetyl trimethyl ammonium bromide (CTAB) [8]. Among them, much interest has been focused on the effect of CTAB because it is easily made into a clear solution. So, a number of researchers have paid attention on controlling the ZnO shape via a CTAB-modified precursor solution. A variety of one-dimensional (1-D) ZnO structures such as rod-like, whisker-like, branch rod-like and sword-like shapes were prepared from different zinc salts and precipitating agents by a hydrothermal method at a high reaction temperature (>150 °C) [9-16]. Furthermore, many researchers also presented the influence of CTAB on the formation of ZnO by other techniques. Ishikawa *et al.* [17] showed that a rod shape was formed by a pulse laser ablation technique at low temperature (40, 60 and 80 °C) and a short reaction time (40 minutes) while Ni *et al.* [18] reported that a columnar structure was shaped by a microwave irradiation method. Noticeably, only a few studies displayed the role of CTAB in the size and shape control of ZnO particles by a precipitation method so far. For example, a spherical ZnO shape was formed from the reaction of CTAB-assisted $ZnCl_2$ and ammonia solution at room temperature with stirring for 96 h [19]. Meanwhile, a flake shape was formed if a CTAB-modified NH_4OH solution was mixed with a $ZnCl_2$ solution and this mixed solution was agitated for 450 h [20]. Moreover, Chen *et al.* [8] reported that a flower-like structure was shaped when a mixture of $ZnSO_4.7H_2O$ and NaOH solution was aged in the oven at 60 °C for 14 h.

In this study, we report the effect of CTAB on the formation of 1-D ZnO structures via a precipitation route from a $Zn(CH_3COO)_2.2H_2O$ precursor solution when hexamethylene tetramine (HMTA) and NaOH solution were used as precipitating agent and the mixed solutions

*Corresponding author:
Tel : +66 74 28 82 50
Fax: +66 74 21 87 01
E-mail: ssuwanboon@yahoo.com

were stirred continuously at 70 °C for 3 h. The authors hope that the results obtained can complete the missing information on the preparation of ZnO nanoparticles by a precipitation method when CTAB was selected as the capping agent.

Experimental

Materials

All chemical agents employed in these experiments were analytical grade and they were used without further purification. The chemical agents were composed of zinc acetate dihydrate ($Zn(CH_3COO)_2.2H_2O$, Fluka), hexamethylene tetramine (HMTA, $C_6H_{12}N_4$, Fluka), cetyl trimethyl ammonium bromide (CTAB, $C_{19}H_{42}BrN$, Fluka) and sodium hydroxide (NaOH, Carlo Erba).

Synthesis of branch rod-like ZnO particles

0.16 mol NaOH was dissolved in 100 ml of distilled water and each of the solutions was stirred at room temperature for 10 minutes until a clear solution was obtained. Then, 0.01 and 0.02 mol CTAB was added separately into the previous NaOH solutions and they were stirred continuously for 1 h. Finally, 0.02 mol $Zn(CH_3COO)_2.2H_2O$ that was dissolved in 100 ml of distilled water was added dropwise into the CTAB-assisted NaOH solutions. White precipitates were formed and they were still stirred at a constant temperature of 70 °C for 3 h. After the precipitates were cooled to room temperature, they were filtered, rinsed with distilled water several times and ethanol, then collected and calcined at 600 °C in air for 1 h.

Synthesis of columnar hexagonal-like ZnO particles

0.16 mol HMTA was dissolved in 100 ml of distilled water and each of the solutions was stirred at room temperature for 10 minutes until clear solutions were obtained. The other processes were followed as in preparing branch rod-like ZnO particles.

Characterization

The structural and phase formation were identified by an X-ray diffractometer (XRD, X'Pert MPD, PHILIPS). The morphological study was evaluated by a scanning electron microscope (SEM, JSM-5800LV, JEOL). The molecular structure was characterized by IR spectroscopy (Spectrum BX, Perkin Elmer). The optical absorbance was determined by a UV-vis spectrophotometer (UV-vis 2450, Shimadzu) and room temperature photoluminescence (PL) spectra were measured by a luminescence spectrometer (LS/55, PerkinElmer).

Results and Discussion

Structural study

The phase identification of all samples was, first of all, studied in order to examine the purity of the calcined samples. Fig. 1 showed that the XRD patterns of all the

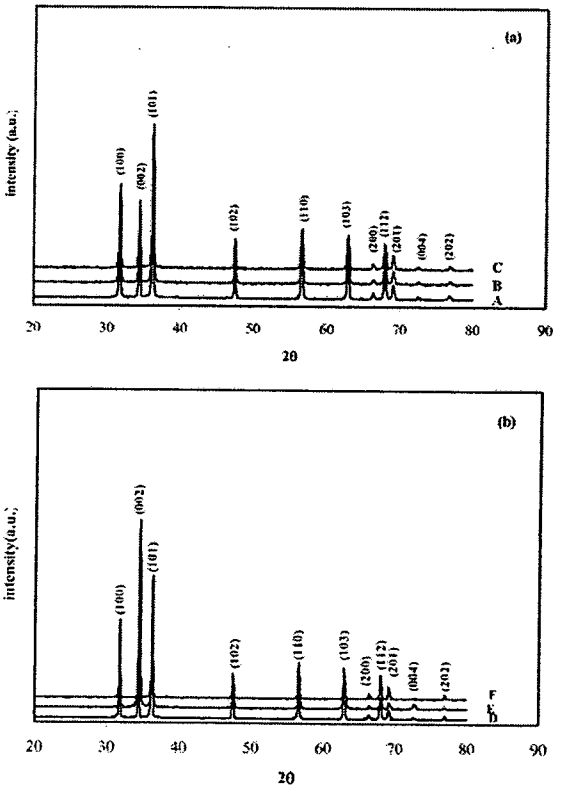

Fig. 1. XRD patterns of calcined ZnO particles prepared from CTAB-modified base solutions (a) NaOH solution with 0 (A), 0.01 (B) and 0.02 (C) mol CTAB as well as (b) HMTA solution with 0 (D), 0.01 (E) and 0.02 (F) mol CTAB.

samples indexed only as the diffraction pattern of the hexagonal or wurtzite structure without any diffraction peaks of a secondary phase neither $Zn(OH)_2$ nor CH_3COONa in accordance with the JCPDS database 36-1451. Applying to the Debye-Scherrer formula [21], the average crystallite size was calculated and the results are presented in Table 1.

It is noteworthy that the type of precipitating agent and concentration of capping agent (CTAB) are the crucial parameters in this system. It is evident that the crystallite size decreased gradually as a function of the CTAB concentration. In the crystallization process, it could be considered that CTAB played an important role in diminishing the crystallite size by two different ways. Firstly, CTAB is a cationic surfactant and it can ionize completely in water. CTA^+ could then adsorb on the surface of ZnO nuclei, giving rise to a reduction of the surface energy [22]. As a matter of fact, the surface energy of a material relates closely to the grain boundary energy. Usually, the grain boundary energy is assumed to be about 1/3 of the surface energy of a material. From this point of view, it could be concluded that the grain boundary energy decreases if the surface energy decreases, resulting in a reduction of the driving force for particle growth [23]. Secondly, The CTA^+ ions could interact with a unit growth $[Zn(OH)_4]^{2-}$ after the zinc precursor solution was introduced

Table 1. Information of the synthetic conditions and ZnO particles obtained

precipitating agent	CTAB concentration (mol)	Crystallite size (nm)	Particle size (diameter) (nm)	Particle shape
HMTA	0	49.48	501	Columnar hexagonal
	0.01	47.17	473	
	0.02	45.41	436	
NaOH	0	46.81	274	Branch rod
	0.01	42.85	202	
	0.02	41.26	148	

into the CTAB-assisted NaOH and CTAB-assisted HMTA solutions due to the electrostatic interaction and then the strong interaction between positively charged CTA^+ and negatively charged plane of the ZnO nuclei brought about either the inhibition of ZnO dissolution (that could promote the crystalline growth) or inhibition of the adsorption of dissolved Zn species on the ZnO particle. So, the growth process was suppressed and a smaller crystallite size is formed as a higher CTAB concentration was used [17]. The reduction of crystallite size does not only depend upon CTAB concentration, but also the type of precipitating agent used. It is evident that a smaller crystallite size was obtained when an aqueous NaOH solution was used as the precipitating agent. This result can be explained by a strong reaction of Zn^{2+} and OH^- ions as well as more ZnO nuclei could nucleate due to a different mechanism as described in [24, 25], so a smaller crystallite size was formed.

Fig. 2 shows the IR spectra of calcined ZnO powders prepared from CTAB-modified precursor solutions. Four major absorption peaks were clearly observed in each spectrum. The broad absorption peak located at 3298-3657 cm^{-1} corresponds to the O-H mode. The absorption peak at 2270-2382 cm^{-1} is due to the CO_2 molecule in air. The absorption peak located at 1560-1693 cm^{-1} corresponds to the symmetric C = O stretching mode and the absorption peak located at 460-530 cm^{-1} is the stretching mode of ZnO [26]. Noticeably, the absorption peaks around 2924 and 2854 cm^{-1} because of the stretching modes of methylene

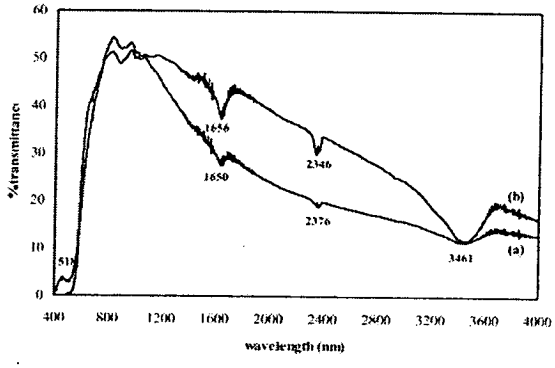

Fig. 2. IR spectra of representative ZnO particles where (a) presence of 0.02 mol CTAB in NaOH solution and (b) presence of 0.02 mol CTAB in HMTA solution.

groups in the long chains of CTAB were not present in the IR spectra. This indicates that CTAB was completely removed from the calcined samples [27].

The particle shape of ZnO precipitated from different precipitating agents was clearly distinct. A columnar hexagonal-like shape was formed when using an aqueous HMTA solution whereas a branch rod-like shape was formed when an aqueous NaOH solution was employed. The dependence of the shape on the precipitating agent can be explained by different paths of the mechanism. Providing NaOH solution as the precipitating agent, $Zn(OH)_2$ precipitates can dissolve under the strong alkaline conditions and then the growth unit $[Zn(OH)_4]^{2-}$ with different growth rate of planes was found to be $v_{(0001)} > v_{(10\bar{1}1)} > v_{(10\bar{1}0)} > v_{(10\bar{1}\bar{1})} > v_{(000\bar{1})}$ were formed in the solution. Finally, the ZnO was precipitated if the ZnO nuclei in the solution reached supersaturation. In this study, we propose that the formation of a branch rod-like shape was similar to the flower-like formation as reported in [22]. By contrast, if the zinc precursor solution was introduced into an aqueous HMTA solution, the particles were shaped differently compared to the NaOH solution. Initially, ZnO nuclei were formed following the mechanism presented in [25]. In this case, the growth rate along the (0001) plane of ZnO nuclei is very much slower than that of the branch rod-like formation. Furthermore, the six side facets of the $(10\bar{1}0)$ family could promote their growth [28], resulting in the formation of columnar hexagonal-like structure as shown in Fig. 3.

Optical study

The optical properties strongly depended upon the particle size and crystallite size of ZnO and the UV absorption of ZnO related to the electronic transition from filled valence states to empty conduction states. The direct optical bandgap of calcined ZnO particles could be evaluated through the well-known relationship as follows [29]:

$$\alpha E = D(E - E_g)^{1/2} \quad (1)$$

where E is the photon energy, α is the absorption coefficient and D is a constant. In this evaluation, the photon energy was calculated by the relationship:

$$E = \frac{1240}{\lambda} \quad (2)$$

where λ is the measured wavelength in nanometers. For the final term, the absorption coefficient could be estimated from:

$$\alpha = A/d \quad (3)$$

where A is the measured absorbance and d' is the thickness of cell.

Fig. 4 showed the extrapolation of the straight line down to $\alpha E = 0$ (where $E = E_g$) for all samples. By using the NaOH solution as the precipitating agent, E_g values of about 3.227, 3.229 and 3.235 eV were obtained as the CTAB concentration was increased from 0 to 0.01 and

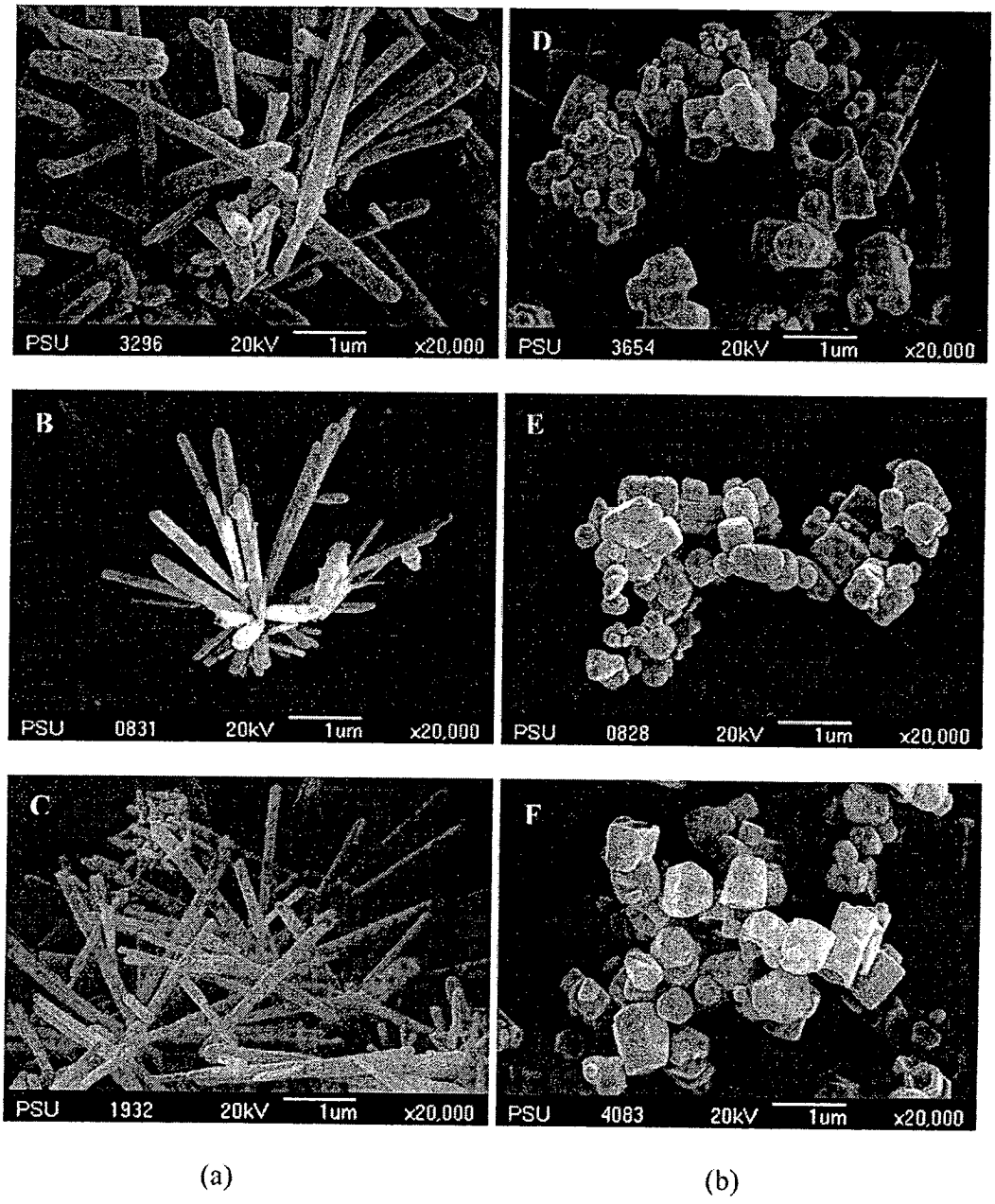

Fig. 3. A SEM images of calcined ZnO particles prepared from CTAB-modified base solutions (a) NaOH solution with 0 (A), 0.01 (B) and 0.02 (C) mol CTAB as well as (b) HMTA solution with 0 (D), 0.01 (E) and 0.02 (F) mol CTAB.

0.02 mole, respectively. Similarly, the E_g values increased from 3.206 to 3.210 and 3.216 eV when HMTA was used as the precipitating agent in the presence of CTAB with an amount of 0, 0.01 and 0.02 mole, respectively. It is clearly seen that the E_g value increased as a function of the CTAB concentration or crystallite size. This was explained by the modification of the band structure, i.e; narrowing of the valence and conduction bands [30]. Regarding the E_g values of ZnO particles precipitated from different bases, the E_g values obtained of the ZnO particles prepared from the NaOH solution were larger than that of the E_g values of the ZnO particles prepared from the HMTA solution. This is because a smaller crystallite size of the ZnO particles was obtained when using the NaOH solution as the precipitating agent in the precipitation process.

Considering the effect of the particle shape on the E_g value, it could be observed that the E_g value of branch rod-like particles with a larger crystallite size (46.81 nm) is wider than that of the E_g value of the columnar hexagonal-like shape particles with a crystallite size of 45.41 nm.

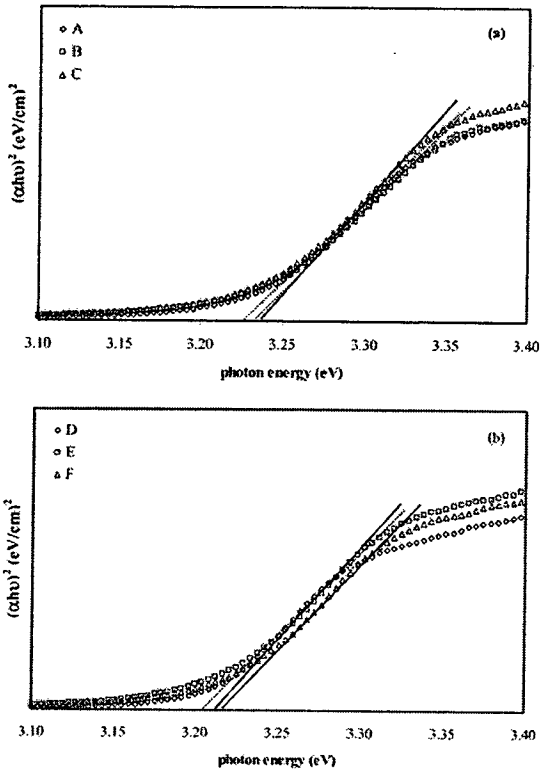

Fig. 4. Evolution of the $(\alpha h\upsilon)^2$ vs. hu curves of calcined ZnO particles prepared from CTAB-modified base solutions (a) NaOH solution with 0 (A), 0.01 (B) and 0.02 (C) mol CTAB as well as (b) HMTA solution with 0 (D), 0.01 (E) and 0.02 (F) mol CTAB.

In summary the particle shape affected directly the E_g value and thus the branch rod-like structure provided a larger E_g value compared to the columnar hexagonal-like structure.

Fig. 5 illustrates the room temperature PL spectra recorded from the branch rod-like ZnO (Fig. 5(a)) and columnar hexagonal-like ZnO (Fig. 5(c)). From Fig. 5, two strong luminescence bands which displayed a UV band and a visible broad band can be observed at about 390 nm and 640 nm, respectively. The emission spectrum of a representative sample was fitted with a Gaussian function and the result showed an emission peak at about 390 nm in the UV region. This peak is attributed to the direct recombination of excitons through an exciton-exciton collision process or exciton annihilation which is a characteristic near the band gap of ZnO. The broad band in the visible region showed three peaks centered at about 510, 620 and 730 nm. Herein, it could be said that the emission peaks centered at 390, 510 and 620 nm are basic PL emissions [31, 32] and the peak centered at about 730 nm is an overtone emission at about 390 nm [33]. An explanation of the emission in the visible region is still an important issue. Nevertheless, it is as yet not understood clearly. Many reports [34-37] considered that oxygen vacancies could be responsible for the visible emission. In this study, the peak at about 510 nm (green emission) is associated with an optical transition in a singly ionized oxygen vacancy and the emission peak located at about 620 nm (yellow emission) is attributed to a single negatively charged interstitial oxygen ion [38]. It is noteworthy that the room temperature PL intensity of ZnO particles prepared from

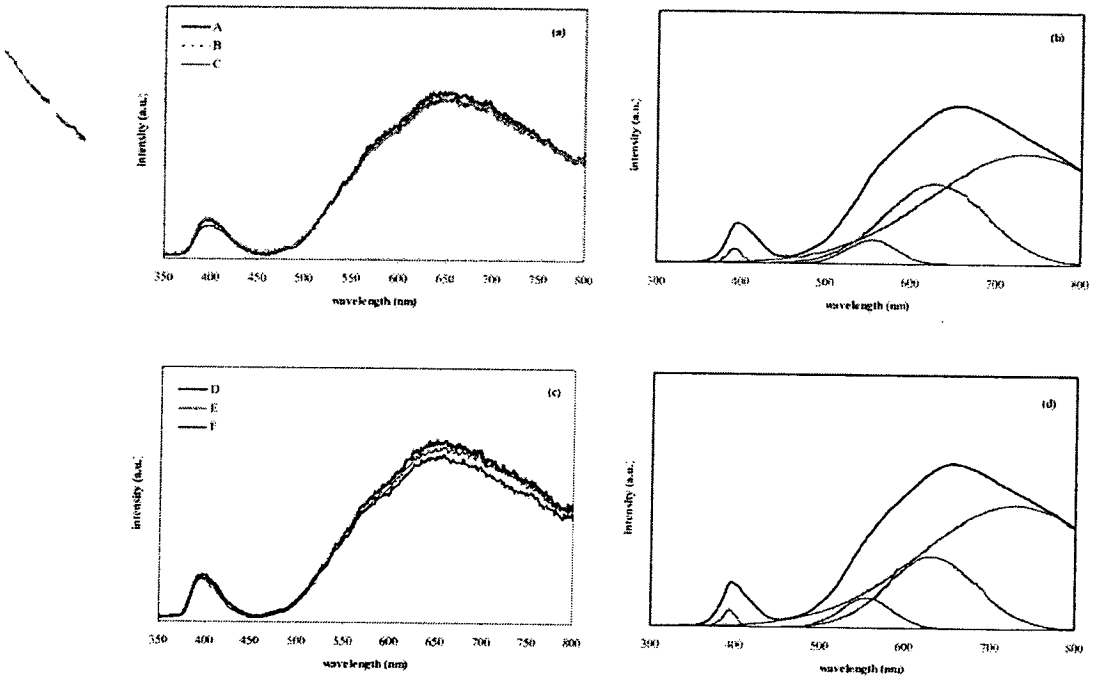

Fig. 5. (a) Room temperature PL spectra of calcined ZnO particles prepared from NaOH solution with 0 (A), 0.01 (B) and 0.02 (C) mol CTAB, (b) PL emission of sample C fitting with Gaussian function, (c) Room temperature PL spectra of calcined ZnO particles prepared from HMTA solution with 0 (D), 0.01 (E) and 0.02 (F) mol CTAB and (d) PL emission of sample F fitting with Gaussian function.

the CTAB-modified zinc precursor solution is lower than that of the PL intensity of ZnO particles prepared from the solution without any addition of CTAB, indicating that CTAB could help in reducing the defects in ZnO crystals.

Conclusions

Branch rod-like and columnar hexagonal-like ZnO particles were successfully fabricated by a precipitation method at low temperature. The type of precipitating agent strongly influenced the particle shape and crystallite size. A smaller crystallite size and branch rod-like shape were obtained when an aqueous NaOH solution was used whereas a columnar hexagonal-like shape with a larger crystallite size was obtained when using an aqueous HMTA solution as the precipitating agent. The shape and size of ZnO particles directly affected the E_g value obtained. A wider E_g value was obtained from the smaller crystallite size and branch rod-like shape. The room temperature PL emission showed four major peaks centered at about 390, 510, 620 and 730 nm when fitted with a Gaussian function. The PL intensity in the visible region decreased as a function of the CTAB concentration, indicating that the defects in the ZnO structure were decreased as CTAB was introduced into the precursor solution.

Acknowledgements

This research is supported by Thailand Research Fund (TRF) under the contract number MRG5280125 and the authors also would like to acknowledge the Center for Innovation in Chemistry (PERCH-CIC), Commission on Higher Education, Ministry of Education.

References

1. C.D. Lokhande, P.M. Gondkai, R.S. Mane, V.R. Shinde and S.H. Han, J. Alloys Compd. 475[1-2] (2009) 304-311.
2. W.C. Shih, H.Y. Su and M.S. Wu, Thin Solid Films. 517[11] (2009) 3378-3381.
3. M. Sugano, M. Tsubosaka, S. Shimizu, M. Fujita, T. Fukumoto, K. Hirano and K. Mashimo, Energy Fuels. 22[3] (2008) 1986-1990.
4. E. Ekambaram, Y. Iikubo and A. Kudo, J. Alloys Compd. 433[1-2] (2007) 237-240.
5. T. Ratana, P. Amornpitoksuk, T. Ratana and S. Suwanboon, J. Alloys Compd. 470[1-2] (2009) 408-412.
6. A.K. Singh, V. Viswanath and V.C. Janu, J. Lumin. 129[8] (2009) 874-878.
7. M. Bitenc and Z.C. Orel, Mater. Res. Bull. 44[2] (2009) 381-387.
8. J. Chen, Y. Hu and X. Zheng, Colloids Surf., A: Physicochem. Eng. Aspect. 313-314 (2008) 576-580.
9. H. Hou, Y. Xie and Q. Li, Solid State Sci. 7[1] (2005) 45-51.
10. L. Wu, Y. Wu and W. Lu, Physica E. 28[1] (2005) 76-82.
11. Y.H. Ni, X.W. Wei, X. Ma and J.M. Hong, J. Crys. Growth. 283[1-2] (2005) 48-56.
12. F. Li, L. Hu, Z. Li and X. Huang, J. Alloys Compd. 465[1-2] (2008) L14-L19.
13. H.J. Zhai, W.H. Wu, F. Lu, H.S. Wang and C. Wang, Mater. Chem. Phys. 112[3] (2008) 1024-1028.
14. J. Xu, Y. Zhang, Y. Chen, Q. Xiang, Q. Pan and L. Shi, Mater. Sci. Eng., B. 150[1] (2008) 55-60.
15. Y.H. Ni, X.W. Wei, J.M. Hong and Y. Ye, Mater. Sci. Eng., B. 121[1-2] (2005) 42-47.
16. X. Jiaqiang, C. Yuping, L. Yadong and S. Jianain, J. Mater. Sci. 40 (2005) 2919-2921.
17. Y, Ishikawa, Y. Shimizu, T. Sasaki and N. Koshizaki, J. Colloid Interface Sci. 300[2] (2006) 621-615.
18. Y. Ni, S. Yang, J. Hong, P. Zhen, Y. Zhou and D. Chu, Scr. Mater. 59[1] (2008) 127-130.
19. Y.D. Wang, C.L. Ma, X.D. Sun and H.D. Li, Inorg. Chem. Commun. 5[10] (2002) 751-755.
20. Y.D. Wang, S. Zhang, C.L. Ma and H.D. Li, J. Lumin. 126[2] (2007) 661-664.
21. S. Suwanboon, P. Amornpitoksuk, A. Haidoux and J.C. Tedenac, J. Alloys Compd. 462[1-2] (2008) 335-339.
22. H. Zhang, D. Yang, Y. Ji, X. Ma, J. Xu and D. Que, J. Phys. Chem. B. 108[13] (2004) 3955-3958.
23. R.W. Kelsall, I.W. Hamley and M. Geoghegan, in "Nanoscale Science and Technology" (Chichester, West Sussex, 2005) p. 265.
24. X. Ma, H. Zhang, Y. Ji, J. Xu, and D. Yang, Mater. Lett. 59[26] (2005) 3393-3397.
25. D. Polsongkram, P. Chamninok, S. Pukird, L. Chow, O. Lupan, G. Chai, H. Khallaf, S. Park and A. Schulte, Physica B. 403[19-20] (2008) 3713-3717.
26. J.H. Zeng, B.B. Jin and Y. F. Wang, Chem. Phys. Lett. 472[1-3] (2009) 90-95.
27. T. Dai, X. Yang and Y. Lu, Nanotechnology. 17[12] (2006) 3028-3034.
28. Q. Ahsanulhaq, J. H. Kim, N. K. Reddy and Y. B. Hahn, J. Ind. Eng. Chem. 14[5] (2008) 578-583.
29. S. Dutta, S. Chattopadhyay, A. Sarkar, M. Chakrabarti, D. Sanyal and D. Jana, Prog. Mater. Sci. 54[1] (2009) 89-136.
30. M. Chakrabarti, S. Dutta, S. Chattapadhyay, A. Sarkar, D. Sanyal and A. Chakrabarti, Nanotechnology. 15[12] (2004) 1792-1796.
31. K. Vanheusden, W.L. Warren, C.H. Seager, D.R. Tallant, J.A. Voigt and B.E. Gnade, J. Appl. Phys. 79[10] (1996) 7983-7990.
32. O.F. Schirmer and D. Zwingel, Solid State Commun. 8[19] (1970) 1559-1562.
33. Y. Hu, and H.J. Chen, Mater. Res. Bull. 43[8-9] (2008) 2153-2159.
34. B. Ha, H. Ham, and C.J. Lee, J. Phys. Chem. Solids. 69[10] (2008) 2453-2456.
35. M.K. Patra, M. Manoth, V.K. Singh, G.S. Gowd, V.S. Choudhry, S.R. Vadera and N. Kumar, J. Lumin. 129[3] (2009) 320-324.
36. S. Sepulveda-Guzman, B. Reeja-Jayan, E.D.L. Rosa, A. Torres-Castro, V. Gonzalez-Gonzalez and M. Jose-Yacaman, Mater. Chem. Phys. 115[1] (2009) 172-178.
37. M. Bitenc, P. Podbrsceek, Z.C. Orel, M.A. Cleveland, J.A. Paramo, R.M. Peters and Y.M. Strzhemechny, Cryst. Growth Des. 9[2] (2009) 997-1001.
38. M. Wang, K.E. Lee, S.H. Hahn, E.J. Kim, S. Kim, J.S. Chung, E.W. Shin and C. Park, Mater. Lett. 61[4-5] (2007) 1118-1121.

Journal of Ceramic Processing Research. Vol. 11, No. 5, pp. 547~551 (2010)

J O U R N A L O F
Ceramic Processing Research

The dependence of optical properties on the morphology and defects of nanocrystalline ZnO powders and their antibacterial activity

Sumetha Suwanboon[a,*], Pongsaton Amornpitoksuk[b], Phuwadol Bangrak[c], Apinya Sukolrat[d] and Nantakan Muensit[e]

[a]*Department of Materials Science and Technology, Faculty of Science, Prince of Songkla University, Hat Yai, Songkhla, 90112, Thailand*

[b]*Department of Chemistry and Center for Innovation in Chemistry, Faculty of Science, Prince of Songkla University, Hat Yai, Songkhla, 90112, Thailand*

[c]*School of Science, Walailak University, Nakhon Si Thammarat, Thailand, 80161, Thailand*

[d]*Scientific Equipment Center, Prince of Songkla University, Hat Yai, Songkhla, 90112, Thailand*

[e]*Department of Physics, Faculty of Science, Prince of Songkla University, Hat Yai, Songkhla, 90112, Thailand*

Nanocrystalline ZnO powders in a variety of shapes were synthesized through an easy precipitation method. Zinc salts, stabilizers and precipitating agents strongly affected the formation of the ZnO structure. The band gap value depended closely upon the amount of defects in various ZnO structures. The largest band gap value of 3.228 eV was obtained from ZnO nanorods with a crystallite size of 42 nm and a relative defect parameter of 0.099. The nanocrystalline ZnO particles can damage only *S. aureus*.

Key words: Precipitation, Defects, Optical properties, ZnO, Antibacteria.

Introduction

In recent years, much attention has been focused on the fabrication of ZnO nanostructures because of their unique physical and chemical properties. Naturally, ZnO is an n-type II-VI semiconductor with a wide band gap of 3.37 eV and a large exciton binding energy of 60 meV [1]. Therefore, ZnO can be used in many potential applications such in optoelectronic devices [2, 3], as rubber additives [4, 5], and for photocatalytic [6], antibacterial [7] and biomedical applications [8]. It has been well known that the properties of ZnO closely depend upon its size and shape. Thus, the strategy in morphological control has been concentrated in order to gain ZnO particles of various shapes such as spherical particles [9, 10], nanorods [1], nanowires [11], nanoflowers [12], and a porous ZnO structure [13] etc. To date, many techniques have been used to make ZnO nanostructures [14-18]. However, a precipitation method is nowadays a fashionable route because it is an easy method to control the precursor solution by a stabilizer as well as a high temperature and sophisticated equipments are not required. As far as we know, neither the formation of a flower-like ZnO structure via a TOA-assisted NH_4OH solution nor the formation of a porous ZnO structure through a CTAB-modified NaOH solution have been reported as yet. Therefore, we, herein, report a simple approach to prepare the ZnO nanostructures with different shapes from the CTAB and TOA-modified precipitating agent solutions and we also investigated the dependence of the band gap energy on the morphology and defects as well as the antibacterial activity towards *Staphylococcus aureus* and *Escherichia coli* was tested by an agar well diffusion assay.

*Corresponding author:
Tel : +66-74-28-8250
Fax: +66-74-28-8395
E-mail: ssuwanboon@yahoo.com

Experiment

Materials

The chemicals used in these experiments were analytical grade and they were used as received. Zinc acetate dihydrate ($Zn(CH_3COO)_2{\cdot}2H_2O$), zinc nitrate hexahydrate ($Zn(NO_3)_2{\cdot}6H_2O$), cetyltrimethyl ammonium bromide or CTAB ($C_{19}H_{42}BrN$) and trioctylamine or TOA ($C_{24}H_{51}N$) were purchased from Fluka. Ammonia solution (25% NH_4OH) and sodium hydroxide (NaOH) were supplied by Carlo Erba. Oxalic acid dihydrate ($C_2H_2O_4{\cdot}2H_2O$) was purchased from MERCK.

Preparation of ZnO nanorods (sample code: A)

6.4 g of NaOH (0.16 mol) was first dissolved in 100 ml of distilled water in a 600-ml conical flask. 7.2892 g of CTAB (0.02 mol) was then added into an aqueous NaOH solution and this solution was stirred continuously for 1 h until a homogeneous solution was obtained. 4.39 g of

$Zn(CH_3COO)_2{\cdot}2H_2O$ (0.02 mol) that was dissolved in 100 ml of distilled water, was finally dropped slowly into a CTAB-assisted NaOH solution. White precipitates were formed and they were heated at 70 °C for 1 h. The precipitates were filtered after being cooled and they were then rinsed with 300 ml of distilled water and 50 ml of absolute ethanol. After that they were dried at room temperature and calcined at 600 °C in air for 1 h.

Preparation of platelet-like ZnO nanoparticles (sample code: B)

1.6 g of NaOH (0.04 mol) was used in these experiments and the other processes were followed as in preparing the ZnO nanorods.

Preparation of ZnO nanoflowers (sample code: C)

6 ml of NH_4OH was first dissolved in 94 ml of distilled water in a 600-ml conical flask. 4.36 ml of TOA was then pipetted into a previous solution and this solution was further stirred at room temperature for 30 minutes. Finally, 4.39 g of $Zn(CH_3COO)_2{\cdot}2H_2O$ (0.02 mol) that was dissolved in 100 ml of distilled water, was added dropwise into a TOA-assisted NH_4OH solution. The other processes were followed as in preparing ZnO nanorods.

Preparation of a porous ZnO structure (sample code: D (without CTAB) and E (modified with CTAB)

20.1712 g of $C_2H_2O_4{\cdot}2H_2O$ (0.16 mol) was first dissolved in 100 ml of distilled water in each 600-ml conical flask for 1 h. 7.2892 g of CTAB (0.02 mol) was then added into an aqueous $C_2H_2O_4{\cdot}2H_2O$ solution while another $C_2H_2O_4{\cdot}2H_2O$ solution did not introduce the CTAB and these solutions were stirred continuously for 1 h until the homogeneous solutions were obtained. 5.9496 g of $Zn(NO_3)_2{\cdot}6H_2O$ (0.02 mol) that was dissolved in 100 ml of distilled water, was finally added dropwise into the $C_2H_2O_4{\cdot}2H_2O$ solution and the CTAB-assisted $C_2H_2O_4{\cdot}2H_2O$ solution. White precipitates were formed and they were stirred at room temperature for 1 h. The precipitates were filtered and they were then rinsed with 300 ml of distilled water and 50 ml of absolute ethanol. After that they were dried at room temperature and calcined at 600 °C in air for 1 h.

Sample characterizations

The structural and phase formation were identified by an X-ray diffractometer (XRD, X'Pert MPD, PHILIPS). The morphological study was evaluated by a scanning electron microscope (SEM, JSM-5800LV, JEOL) and the optical absorbance was determined by a UV-Vis spectrophotometer (UV-Vis 2450, Shimadzu).

Test of antibacterial activity

Antibacterial tests were performed by an agar well diffusion assay using a gram-positive bacterium *S. aureus* and gram-negative bacterium *E. coli* as indicator strains. The two species of bacteria grown individually on nutrient agar plates at 37 °C for 16-18 h were resuspended in 0.85% sterile saline equivalent to a turbidity of standard McFarland No. 0.5 with approximate 1.5×10^8 colony forming units/ml (CFU/ml). The suspension of testing bacteria was spread on the Mueller-Hinton agar plate and left at room temperature for 5 minutes so as to allow the moisture from the inocula to absorb into the medium. Wells were punched in the agar with a sterile cock-borer of 9 mm diameter. The ZnO suspensions (2.5 mg/ml) were filled directly into the wells of the agar plates inoculated with indicator bacteria. The agar plates were left at room temperature for 15 minutes and then incubated at 37 °C for 16 h and the diameters of the inhibition zones were finally measured in millimetre.

Results and Discussion

Structural study

The calcined ZnO samples were identified by the XRD technique and the results are shown in Fig. 1

The XRD patterns of all samples were in good agreement with the pattern of the ZnO standard with a space group of $P6_3mc$ and lattice parameters: $a = 0.3250$ and $c = 0.5207$ nm according to the JCPDS number of 36-1451. Therefore, it could be concluded that the calcined samples are a pure ZnO phase. Based on the XRD results, the average crystallite size of ZnO was determined by Scherrer's formula [19] ($D = k\lambda/\beta\cos\theta$, where D is the average crystallite size, k is a constant equal to 1, λ is the wavelength of the X-rays used, β is a line width in radians at half maximum intensity and θ is the Bragg angle). The calculated crystallite sizes are given in Table 1.

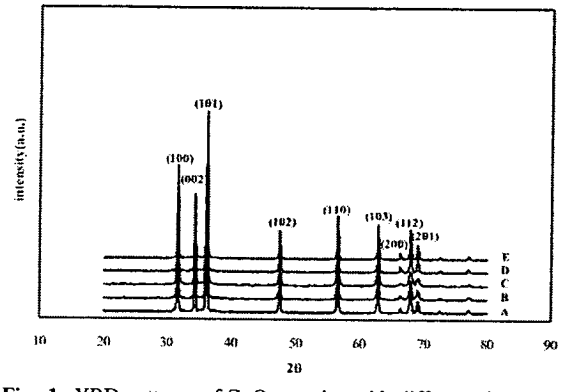

Fig. 1. XRD patterns of ZnO samples with different shapes A: nanorod, B: platelet, C: nanoflower, D and E: porous structure.

Table. 1. The data of structural and optical properties of ZnO samples

sample code	crystallite size (nm)	lattice parameter (nm)		E_g (eV)	particle shape	I/slope
		a	*c*			
A	42	0.3253	0.5211	3.228	rod	0.099
B	41	0.3254	0.5213	3.171	platelet	0.129
C	34	0.3254	0.5212	3.174	flower	0.111
D	46	0.3254	0.5212	3.198	porous	0.127
E	54	0.3254	0.5213	3.204	porous	0.072

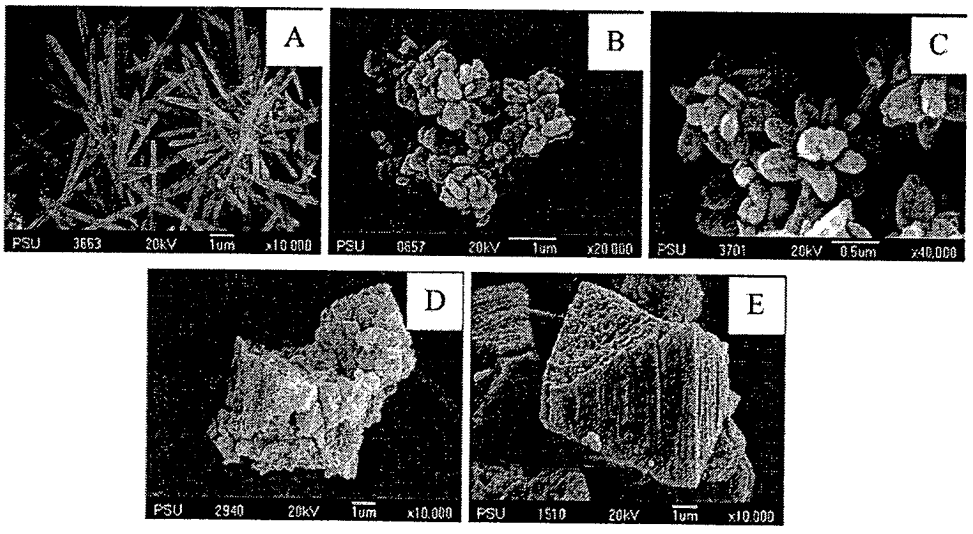

Fig. 2. SEM images of calcined ZnO samples with different shapes.

It was evident that the crystallite size of calcined ZnO samples strongly depended upon the conditions used. The smallest crystallite size of about 34 nm was observed when TOA and ammonia solution were used as a capping agent and a precipitating agent, respectively. Not only the crystallite size, but also the particle shape was influenced from the conditions selected as seen in the SEM images in Fig. 2.

It was clearly seen that different shapes of ZnO nanostructures were formed when different preparation conditions were used in this study. Rod structures (sample A) were shaped when 0.16 mol NaOH solution was used while the platelet-like shape (sample B) was formed when the amount of NaOH was reduced to 0.04 mol. Here, the dependence of ZnO shape on the concentration of the aqueous NaOH solution could be explained by different growth rate of crystal planes. Under a strong alkaline solution (sample A), $Zn(OH)_2$ was formed and was completely dissolved to $Zn(OH)_4^{2-}$. The $Zn(OH)_4^{2-}$ could act as a growth unit with different growth rates of the planes as follows [20]:

$$v_{(0001)} > v_{(\bar{1}0\bar{1}\bar{1})} > v_{(\bar{1}010)} > v_{(\bar{1}011)} > v_{(000\bar{1})}.$$

If the degree of supersaturation exceeds the critical value, the ZnO nuclei started to nucleate in the solutions and this was followed with a subsequent growth in the form of a rod structure under the driving force of the surface energy, electrostatic force [21] etc. Furthermore, the $N(CH_3)_3^+$ or CTA^+ groups could encapsulate on the side faces of ZnO, giving rise to a rapid growth along the *c*-axis and thus a smaller rod was shaped. On the other hand, a platelet-like shape was formed with a lower NaOH concentration (0.04 mol). It is proposed that the $Zn(OH)_2$ could not dissolve completely and the $Zn(OH)_2$ played an important role in controlling the growth of the platelet-like ZnO structure. In this case, the growth along the *c*-axis was prevented and the growth could occur along the slowest growth rate of the $(000\bar{1})$ plane and the side faces. To date, it has been well known that an explanation of the growth process and mechanism for ZnO formation has not been clear enough. However, under a mild alkaline solution with a presence of CTAB, a growth process of ZnO via the following reactions could be accepted [21, 22]:

$$Zn^{2+} + 2OH^- + CTA^+ \leftrightarrow Zn(OH)_2\text{-}CTA^+ \quad (1)$$

$$Zn(OH)_2\text{-}CTA^+ \leftrightarrow ZnO\text{-}CTA^+ + H_2O \quad (2)$$

$$ZnO\text{-}CTA^+ \overset{\Delta}{\leftrightarrow} ZnO \quad (3)$$

Owing to the smaller solubility of ZnO compared to $Zn(OH)_2$, the $Zn(OH)_2$ consequently tended to be transformed into ZnO. In contrast, ZnO was formed under a strong alkaline solution via the following reactions [23]:

$$Zn^{2+} + 2OH^- + CTA^+ \leftrightarrow Zn(OH)_2\text{-}CTA^+ \quad (4)$$

$$Zn(OH)_2\text{-}CTA^+ + 2OH^- \leftrightarrow Zn(OH)_4^{2-}\text{-}CTA^+ \quad (5)$$

$$Zn(OH)_4^{2-}\text{-}CTA^+ \rightarrow ZnO\text{-}CTA^+ + H_2O + 2OH^- \quad (6)$$

$$ZnO\text{-}CTA^+ \overset{\Delta}{\rightarrow} ZnO \quad (7)$$

Considering the mechanism for formation of the flower-shaped ZnO structure (sample C), it has been found that an organic amine and an ammonium solution were a key parameter influencing the formation of a flower-like structure [24, 25]. Here, TOA could primarily adsorb on the (0001) plane of ZnO nuclei and the growth along (0001) plane or the *c*-axis was greatly retarded which was similar to the effect of TEA [26, 27]. Moreover, the adsorption of TOA on the (0001) plane was not uniform and the adsorption always deviated from the center of the plane. So, its shape was similar to the petals. In this study, the ZnO formation can be depicted by the following reactions:

$$NH_3 + H_2O \leftrightarrow NH_3.H_2O \leftrightarrow NH_4^+ + OH^- \quad (8)$$

$$Zn^{2+} + 2OH^- + TOA \leftrightarrow Zn(OH)_2\text{–}TOA \quad (9)$$

$$Zn(OH)_2\text{–}TOA + 2OH^- \leftrightarrow Zn(OH)_4^{2-}\text{–}TOA \quad (10)$$

$$Zn(OH)_4^{2-}\text{–}TOA \rightarrow ZnO\text{-}TOA + H_2O + 2OH^- \quad (11)$$

$$ZnO\text{-}TOA \xrightarrow{\Delta} ZnO \quad (12)$$

For construction of a porous ZnO structure, it was clearly observed that CTAB did not affect the shape of ZnO under a strong acidic solution as clearly seen from SEM images for samples D and E in Fig. 2. The SEM images showed that a porous ZnO structure was constructed with well-aligned spherical particles with a size of about 200 nm. In this study, a porous ZnO structure was formed via the ZnC_2O_4 intermediate that can be described by the following reactions [28]:

$$Zn^{2+} + C_2O_4^{2-} \rightarrow ZnC_2O_4.2H_2O \quad (13)$$

$$ZnC_2O_4.2H_2O + 1/2O_2 \xrightarrow{\Delta} ZnO + 2CO_2 + 2H_2O \quad s(14)$$

Optical study

As far as ZnO nanomaterial is concerned, the investigation of its optical properties has been of interest because ZnO has a great potential in many applications. In this study, the absorbance of all calcined samples was measured and the results are presented in Fig. 3(a).

The ZnO samples prepared in these experiments showed a highly transparent mode in the visible region and the absorption edge of all samples was lower than 400 nm depending upon their shape and size. To estimate the band gap value (E_g), the curve of $(\alpha h\upsilon)^2$ versus $h\upsilon$ or Kubelka-Munk model [29] was plotted as displayed in Fig. 3(b). The extrapolation of the straight line down to zero on the *x*-axis (where E or $h\upsilon = E_g$) is an E_g value for each sample and the results acquired are given in Table 1. Interestingly, the E_g values are strongly dependent upon the ZnO shape. When alkaline solutions were utilized to germinate the ZnO nuclei, the largest E_g value of 3.228 eV was obtained from the rod structure (sample A) even though it has the largest crystallite size. This might be due to a lower defect concentration in the crystals of ZnO for sample A. To evaluate the amount of defects in ZnO crystals, a curve of $\ln(\alpha)$ versus $h\upsilon$ was plotted and given in Fig. 4 and a reciprocal values that referred to the amount of defects were shown in Table 1.

It is clearly seen that the reciprocal values of the slopes from the linear part are 0.099, 0.129 and 0.111 for samples A, B and C, respectively. Thus, it could be concluded that the ZnO particles with different shapes have a different content of defects and these defects had strongly affected the E_g value. From the results obtained, the E_g value of all samples was smaller than that of the E_g value of a ZnO single cystal (3.37 eV), this might be because the E_g values in these experiments were due to the electronic transition from the filled valence states to energy levels of defects instead of the electronic transition from the filled valence band to the empty conduction band as usual. For this reason, it is reasonable to summarize that a shape with larger crystallite size, but a smaller amount of defects gave a

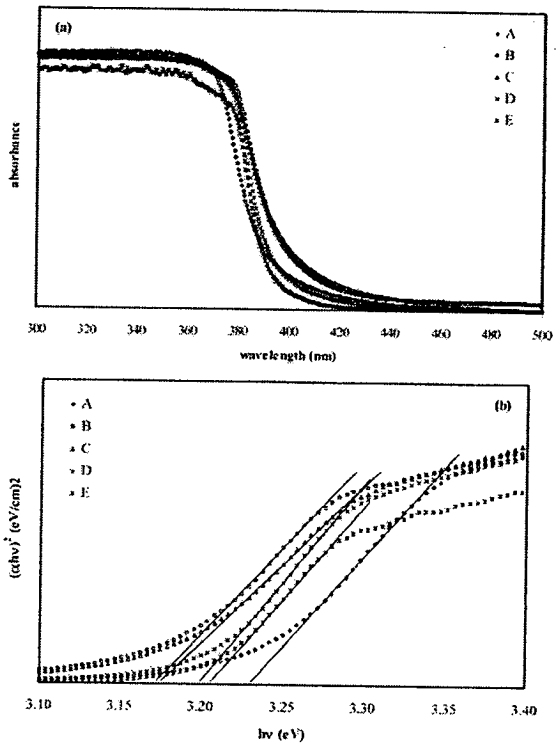

Fig. 3. (a) absorbance spectra, and (b) evolution of the $(\alpha h\upsilon)^2$ vs. $h\upsilon$ curves of the calcined ZnO samples.

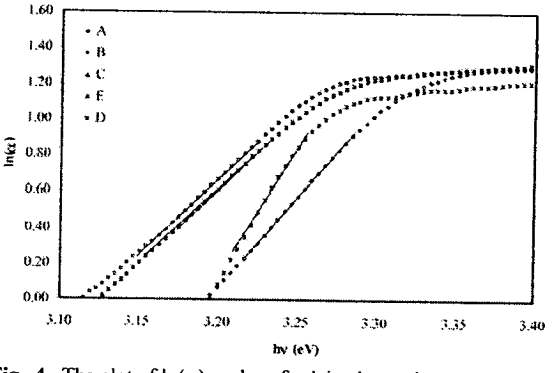

Fig. 4. The plot of $\ln(\alpha)$ vs. $h\upsilon$ of calcined samples.

significantly larger E_g value when the ZnO particles were synthesized by alkaline solutions. Similarly, as the ZnO particles were fabricated under strong acidic conditions (samples D and E), a porous ZnO structure (sample E) with a larger crystallite size, but a smaller amount of defects also showed a larger E_g value.

Antibacterial activity

In this study, the antibacterial activity of ZnO suspension towards *S. aureus* and *E. coli* was tested by an agar well diffusion method and the results are given in Table 2.

From the results obtained, all the ZnO samples synthesized in these experiments can damage only *S. aureus*. It is well known that the gram-positive bacteria (*S. aureus*) and gram-

Table 2. The effect of nanocrystalline ZnO powders on inhibition of *S. aureus* and *E. coli* by an agar well diffusion method

sample code	Inhibition zone diameter (mm)	
	S. aureus	*E. coli*
A	13	none
B	13	none
C	12	none
D	14	none
E	14	none

negative bacteria (*E. coli*) have different basic structures. The outside rigid cell wall of gram-negative bacteria is composed of lipopolysaccharides instead of phospholipids. The lipopolysccharides normally form an extra physical barrier to penetration by the ZnO particles [30]. For this reason, the ZnO can damage better *S. aureus*. The bacterial tests were done under dark conditions, and a possible mechanism for the damage of the bacteria could be due to the penetration of ZnO particles into the membrane cell wall to damage the bacteria from the interior [31]. From this study, the ZnO can penetrate into the cell wall of *S. aureus*, but they can not penetrate into the cell wall of *E. coli* according to the different compositions of membrane cell walls as previously mentioned. Therefore, ZnO particles can damage only *S. aureus*.

Conclusions

Rod-like and platelet-like ZnO structures were shaped from the $Zn(CH_3COO)_2.2H_2O$ and the CTAB-modified NaOH solutions under strong and mild alkaline solutions, respectively. A flower-like ZnO shape was constructed from the $Zn(CH_3COO)_2{\cdot}2H_2O$ and the TOA-modified NH_4OH solutions. A porous ZnO structure was synthesized from $Zn(NO_3)_2{\cdot}6H_2O$ and $C_2H_2O_4{\cdot}2H_2O$ solutions under strong acidic conditions. The value of the optical band gap strongly depended upon the amount of defects and the shape of ZnO particles. The ZnO particles prepared under all conditions in this study could damage only *S. aureus*.

Acknowledgements

The authors would like to acknowledge the financial support from the Thailand Research Fund (TRF) under the contract number MRG5280125 and the Research, Development and Engineering (RD&E) fund through The National Nanotechnology Center (NANOTEC), The National Science and Technology Development Agency (NSTDA), Thailand (Project No. NN-B-22-FN8-19-52-21) to Prince of Songkla University. The authors also would like to acknowledge the Center for Innovation in Chemistry (PERCH-CIC), Commission on Higher Education, Ministry of Education.

References

1. J. Zhao, Z.G. Jin, X.X. Liu and Z.F. Liu, J. Eur. Ceram. Soc. 26[16] (2008) 3745-3752.
2. M. Purica, E. Budianu and E. Rusu, Microelectron. Eng. 51-52 (2002) 425-431.
3. C.Y. Hsu and C.H. Tsang, Sol. Energy Mater. Sol. Cells 92[5] (2008) 530-536.
4. X. Xiao, C. Li, D. Yang, and S. He, Nucl. Instrum. Methods Phys. Res., Sect. B. 266[15] (2008) 3375-3380.
5. M. Sugano, M. Tsubosaka, S. Shimizu, M. Fujita, T. Fukumoto, K. Hirano and K. Mashimo, Energy Fuels. 22[3] (2008) 1986-1990.
6. A. Dodd, A. Mckinley, T. Tsuzuki, and M. Saunders, J. Eur. Ceram. Soc. 29[1] (2009) 139-144.
7. L. Zhang, Y. Ding, M. Povey and D. York, Prog. Nat. Sci. 18[8] (2008) 939-944.
8. D. Guo, C. Wu, H. Jian, Q. Li, X. Wang and B. Chen, J. Photochem. Photobiol., B. 93[3] (2008) 119-126.
9. N. Uekawa, S. Tahii, T. Kojima and K. Kakegawa, Mater. Lett. 61[8-9] (2007) 1729-1734.
10. J.K. Yong, H.K. Hun, L.M. Chang and B.S. Kwang, J. Ceram. Process. Res. 3[3] (2002) 146-149.
11. T.J. Hsueh, C.L. Hsu, S.J. Chang and I.C. Chen, Sens. Actuator B. 126[2] (2007) 473-477.
12. J.M. Jang, C.R. Kim, H. Ryu, M. Razeghi and W.G. Jung, J. Alloys Compd. 463[1-2] (2008) 503-510.
13. J. Zheng, Z.Y. Jiang, Q. Kuang, Z.X. Xie, R.B. Huang and L.S. Zheng, J. Solid State Chem. 182[1] (2009) 115-121.
14. J.E. Rodriguez-Paez, A.C. Caballero, M. Villegas, C. Moure, P. Duran and J.F. Fermandez, J. Eur. Ceram. Soc. 21[7] (2001) 925-930.
15. X.M. Sun, X. Chen, Z.X. Deng and Y.D. Li, Mater. Chem. Phys. 78[1] (2002) 99-104.
16. W.S. Kim, H.W. Kim and N.H. Kim, Physica B. 334[3-4] (2003) 343-346.
17. P.T. Hsieh, Y.C. Chen, K.S. Kao, M.S. Lee and C.C. Cheng, J. Eur. Ceram. Soc. 27[13-15] (2007) 3815-3818.
18. T. Masaki, S.J. Kim, H. Watanabe, K. Miyamoto, M. Ohno and K.H. Kim, J. Ceram. Process. Res. 4[3] (2003) 135-139.
19. T. Ratana, P. Amornpitoksuk, T. Ratana and S. Suwanboon, J. Alloys Compd. 470[1-2] (2009) 408-412.
20. W.J. Li, E.W. Shi, W.Z. Zhong and Z.W. Yin, J. Cryst. Growth. 203[1-2] (1999) 186-196.
21. J. Xie, P. Li, Y. Li, Y. Wang and Y. Wei, Mater. Chem. Phys. 114[2-3] 943-947.
22. Q. Ahsanulhaq, S.H. Kim, J.H. Kim and Y.B. Hahn, Mater. Res. Bull. 43[12] (2008) 3483-3489.
23. R. Yi, N. Zhang, H. Zhou, R. Shi, G. Qiu and X. Liu, Mater. Sci. Eng., B. 153[1-3] (2008) 25-30.
24. M. Epifani, Mater. Lett. 61[14-15] (2007) 3100-3102.
25. Y. Masuda, N. Kinoshita and K. Koumoto, Electrochim. Acta 53[1] (2007) 171-174.
26. P. Li, Y. Wei, H. Liu and X.K. Wang, J. Solid State Chem. 178[3] (2005) 855-860.
27. P. Li, H. Liu, Y.F. Zhang, Y. Wei and X.K. Wang, Mater. Chem. Phys. 106[1] (2007) 63-69.
28. K.G. Kanade, B.B. Kale, R.C. Aiyer and B.K. Das, Mater. Res. Bull. 41[3] (2006) 590-600.
29. T. Rattana, S. Suwanboon, P. Amornpitoksuk, A. Haidoux and P. Limsuwan, J. Alloys Compd. 480[2] (2009) 603-607.
30. P. Lowrie and S. Wells, in "Microbiology and Biotechnology" (Cambridge, 2000) p. 2.
31. L. Zhang, Y. Jiang, Y. Ding, M. Povey and D. York, J. Nanopart. Res. 9 (2007) 479-489.

View Letter

Close

Date: Mar 07, 2011
To: "sumetha suwanboon" ssuwanboon@yahoo.com
From: Pietro Vincenzini councilchair@waceramics.org
Subject: Your SubmissionCERI-D-11-00074R1

Ms. Ref. No.: CERI-D-11-00074R1
Title: Dependence of photocatalytic activity on structural and optical properties of nanocrystalline ZnO powders
Ceramics International

Dear Dr. sumetha suwanboon,

I am pleased to inform you that your paper "Dependence of photocatalytic activity on structural and optical properties of nanocrystalline ZnO powders" has been accepted for publication in Ceramics International.

Thank you for submitting your work to Ceramics International.

Yours sincerely,

Pietro Vincenzini
General Editor
Ceramics International

****

For any technical queries about using EES, please contact Elsevier Author Support at authorsupport@elsevier.com
Global telephone support is available 24/7:
For The Americas: +1 888 834 7287 (toll-free for US & Canadian customers)
For Asia & Pacific: +81 3 5561 5032
For Europe & rest of the world: +353 61 709190

Close

Elsevier Editorial System(tm) for Ceramics International
Manuscript Draft

Manuscript Number: CERI-D-11-00074R1

Title: Dependence of photocatalytic activity on structural and optical properties of nanocrystalline ZnO powders

Article Type: Full Length Article

Keywords: A. Powders: chemical preparation; C. Chemical properties; C. Optical properties; D. ZnO

Corresponding Author: Dr. sumetha suwanboon, Ph.D.

Corresponding Author's Institution: Prince of Songkla University

First Author: sumetha suwanboon, Ph.D

Order of Authors: sumetha suwanboon, Ph.D; pongsaton amornpitoksuk, Ph.D

Abstract: Nanocrystalline ZnO powders were prepared from cetyltrimethylammonium bromide (CTAB)-modified NaOH, NH4OH and (CH2)6N4 solutions. The calcined ZnO powders exhibited a hexagonal structure without any secondary phase. Different shapes of ZnO powders were formed depending on CTAB concentration and type of precipitating agent. As (CH2)6N4 solution was used, rod-like ZnO structure was changed to a spherical shape when CTAB concentration was increased. The widest Eg value of approximately 3.23 eV was obtained from the sample containing the lowest defect concentration. The decolorization efficiency was higher than 90% after irradiating for 90 min and the sample with higher Eg value showed higher decolorization efficiency.

Dependence of photocatalytic activity on structural and optical properties of nanocrystalline ZnO powders

Sumetha Suwanboon[a,*], Pongsaton Amornpitoksuk[b] and Nantakan Muensit[c]

[a]Department of Materials Science and Technology, Faculty of Science, Prince of Songkla University, Hat Yai, Songkhla, 90112 Thailand

[b]Department of Chemistry and Center for Innovation in Chemistry, Faculty of Science, Prince of Songkla University, Hat Yai, Songkhla, 90112 Thailand

[c]Department of Physics, Faculty of Science, Prince of Songkla University, Hat Yai, Songkhla, 90112 Thailand

Abstract

Nanocrystalline ZnO powders were prepared from cetyltrimethylammonium bromide (CTAB)-modified NaOH, NH_4OH and $(CH_2)_6N_4$ solutions. The calcined ZnO powders exhibited a hexagonal structure without any secondary phase. Different shapes of ZnO powders were formed depending on CTAB concentration and type of precipitating agent. As $(CH_2)_6N_4$ solution was used, rod-like ZnO structure was changed to a spherical shape when CTAB concentration was increased. The widest E_g value of approximately 3.23 eV was obtained from the sample containing the lowest defect concentration. The decolorization efficiency was higher than 90% after irradiating for 90 min and the sample with higher E_g value showed higher decolorization efficiency.

Keywords: A. Powders: chemical preparation; C. Chemical properties; C. Optical properties; D. ZnO

Corresponding author:

Asst. Prof. Dr.Sumetha Suwanboon

Department of Materials Science and Technology, Faculty of Science,

Prince of Songkla University, Hat Yai, Songkhla, Thailand, 90112

Tel. 66 74 28 82 50

Fax. 66 74 28 83 95

Email address: ssuwanboon@yahoo.com

1. Introduction

ZnO is normally an *n*-type II-VI semiconductor with a wide band gap of about 3.2 eV and a large exciton binding energy of 60 meV [1]. Consequently, ZnO is one of the candidates for optoelectronic devices [2, 3], solar cell [4] and photocatalytic applications [5]. In recent years, it has been found that ZnO can be synthesized by various routes such as vapor phase [6], sonochemical [7], sol-gel [4] and precipitation [1] methods. Among these methods, precipitation has many advantages over the other methods, for example, it is unsophisticated and a low cost method. Moreover, the morphology of ZnO powders can be controlled easily by using an appropriate surfactant or capping agent such as polyvinylpyrolidone (PVP) [8], polyethylene glycol (PEG) [9], monoethanolamine (MEA), diethanolamine (DEA) or triethanolamine (TEA) [10], polyethylene oxide-block-polypropylene oxide (PEO-b-PPO) copolymer [1] and cetyltrimethylammonium bromide (CTAB) [11]. Furthermore, this method can be used for mass production. It is evident that the desired chemical and physical properties particularly the optical properties and photocatalytic activity strongly related to particle sizes and shapes of ZnO powders. Over the past years, many researchers have reported that ZnO powders have a more powerful photocatalytic reaction than TiO_2 because ZnO powders can absorb larger fractions of the solar spectrum over TiO_2 powders [12]. For this reason, many researchers have focused on synthesis of different morphologies of ZnO powders due to the fact that they displayed the unique properties.

In this study, we report the influence of CTAB concentration on formation of different ZnO morphologies via a precipitation method using sodium hydroxide (NaOH), ammonium hydroxide (NH_4OH) and hexamethylenetetramine ($(CH_2)_6N_4$, HMTA) as a precipitating agent. CTAB was studied because it can dissolve easily in

water and because of the lack of documents the effect of CTAB-modified HMTA solution was not reported. We also compared the effect of CTAB-modified different bases on morphology formation. Furthermore, we also report the effects of particle sizes and shapes on optical properties and photocatalytic activity.

2. Materials and Methods

2.1 Materials

All chemicals were of analytical grade and they were used without further purification. Zinc nitrate hexahydrate ($Zn(NO_3)_2.6H_2O$, Fluka) was used as a zinc source. HMTA ($C_6H_{12}N_4$, Fluka), NH_4OH (Carlo Erba) and NaOH (Carlo Erba) solutions were used as a precipitating agent and CTAB ($C_{19}H_{42}BrN$, Fluka) was used as a capping agent.

2.2 Experimental

To study the effect of each precipitating agent and CTAB concentration, 0.16 mol (6.4 g) NaOH, 0.16 mol (22.43 g) HMTA and 0.04 mol (1.58 ml) NH_4OH were first dissolved in 100 ml of distilled water in a conical flask separately. 0.01 and 0.02 mol (3.64 and 7.28 g) CTAB were then added into each precipitating agent solution and all conditions are presented in Table 1. After that, CTAB-modified precipitating agent solutions were magnetically stirred for 1 h until the homogenous solutions were obtained. 0.02 mol (5.95 g) $Zn(NO_3)_2.6H_2O$ that was dissolved in 100 ml of distilled water, was finally added dropwise into each CTAB-modified precipitating agent solution. White precipitates were formed in the solutions and were heated at 70 °C under a magnetically stirring for 1 h. The precipitates were filtered, rinsed with

distilled water and absolute ethanol, dried at room temperature and finally calcined at 600 °C in air for 1 h.

2.3 Characterizations

The ZnO formation was identified by an X-ray diffraction (XRD, X'Pert MPD, PHILIP) using Cu-K_α radiation (λ = 1.5406 Å). The morphology of ZnO powders was determined by a scanning electron microscope (SEM, JSM-5800LV, JEOL) with an acceleration voltage of 20 kV. The optical absorbance was measured by a UV-Vis spectrophotometer (UV-Vis 2450, Shimadzu) and the room temperature photoluminescence (PL) spectra were recorded by a luminescence spectrometer (LS/55, PerkinElmer).

2.4 Photocatalytic test

The photocatalytic tests on the selected samples for decomposition of methylene blue (MB) in air were performed at ambient temperature. A Pyrex beaker (250 ml) was used as the photoreactor vessels. 150 mg of selected ZnO samples were added in 150 ml of $1x10^{-5}$ M aqueous methylene blue solution. The solutions were magnetically stirred in the dark for 30 min to ensure the establishment of adsorption/desorption equilibrium of methylene blue on the sample surfaces. The solutions were then exposed to a UV light. At given irradiation time intervals (30, 60, 90, 120 and 180 min), 3 ml of each aqueous solution was collected and centrifuged to remove the ZnO powders and was then analyzed on a Lambda 25 UV-Vis spectrometer. The concentration of aqueous methylene blue solution was determined by monitoring the change in the absorbance centered at 665 nm.

3. Results and Discussion

3.1 Effect of synthetic conditions on structural properties

Fig. 1 shows XRD patterns of all calcined samples precipitated from different precipitating agents when CTAB was used as a capping agent. All the diffraction peaks can be indexed only as a diffraction pattern of hexagonal or wurtzite structure in good agreement with the JCPDS 36-1451 (space group $P6_3mc$ and lattice parameters: $a = b = 0.3249(8)$ and $c = 0.5206(6)$ nm), suggesting that the calcined samples are a pure ZnO phase without any secondary phase.

To study the effects of CTAB concentration on the morphology of ZnO, the crystallite size of all calcined ZnO powders was calculated from the XRD results by the Scherrer's formula [13]:

$$D = \frac{k\lambda}{\beta \cos\theta} \quad (1)$$

where D is the crystallite size, k is a shape factor constant ($k = 0.9$), λ is the wavelength of incident X-ray ($\lambda = 0.15406$ nm), θ is the Bragg angle of the diffraction line and β is the full width at half maximum (FWHM) in radian.

It was observed that the crystallite size decreased as CTAB concentration was increased. As we know, CTAB is a cationic surfactant that can ionize completely in water to form a cationic head groups ($N(CH_3)_3^+$) and a long hydrophobic tail. The presence of 0.01 mol (0.025 M) and 0.02 mol (0.05 M) CTAB in the solutions is higher than its critical micelle concentration (0.94 mM), indicating that CTAB acts as a capping agent instead of forming the micelles [14]. For instance, the cationic head groups can be adsorbed on the surface of ZnO by electrostatic interaction and the strong interaction can either suppress the dissolution of ZnO particles or can inhibit the adsorption of dissolved Zn species presented in a bulk solution onto the ZnO

surface. Therefore, the ZnO can not grow any longer and smaller crystallite size was obtained when higher CTAB concentration was used.

The calcined ZnO powders with different shapes and sizes are presented in Fig. 2. The rod-like structure was shaped when NaOH and NH_4OH solutions were used as a precipitating agent. Nevertheless, the particle shape did not alter when CTAB was added into the NaOH and NH_4OH solutions. However, a rod diameter was diminished as a function of CTAB concentration. In contrast, the morphology strongly depended upon CTAB concentration when HMTA solution was used. The rod-like structure was altered to spherical shape when CTAB concentration was increased. To further understand why the different morphologies can form, the growth mechanisms were purposed for each system.

As NaOH solution was used, number of Zn species can form as reported in [15].

$Zn^{2+} + OH^- \leftrightarrow Zn(OH)^+$

$Zn(OH)^+ + OH^- \leftrightarrow Zn(OH)_2$

$Zn(OH)_2 \leftrightarrow Zn^{2+} + 2OH^-$

$Zn(OH)_2 + OH^- \leftrightarrow Zn(OH)_3^-$

$Zn(OH)_2 + 2OH^- \leftrightarrow Zn(OH)_4^{2-}$

$Zn(OH)_4^{2-} \leftrightarrow ZnO + H_2O + 2OH^-$

Under the strong alkaline NaOH solution, $Zn(OH)_4^{2-}$ species acted as a growth unit of ZnO. As a matter of fact, ZnO is a polar crystal, the O^{2-} and Zn^{2+} ions form a tetrahedral unit. Zn and oxygen atoms are arranged alternatively along the *c*-axis and some surfaces are either terminated with Zn^{2+} cations, exhibiting a positive polar plane Zn- (0001) or terminated with O^{2-} anions, exhibiting a negative polar plane O- $(000\bar{1})$. In this study, a pH value of final solution (pH > 13.0) is higher than the point

of zero charge (PZC) of ZnO (~9.5), so the surface of ZnO nuclei is surrounded by negatively-charged species [15] and rod-like structure can grow along the *c*-axis owing to the more rapid growth rate that was found to be $v_{(0001)} > v_{(\bar{1}01\bar{1})} > v_{(\bar{1}010)} > v_{(\bar{1}011)} > v_{(000\bar{1})}$. Via the addition of CTAB in the solutions, the cationic head groups ($N(CH_3)_3^+$) could strongly adsorb on the ZnO facets by electrostatic interaction, giving rise to a further growth along the *c*-axis [17].

In the case of HMTA solution was used, a pH value of final solution is 8.8. Under this condition, rod-like ZnO structure was changed evidently to a spherical shape when the solution was modified by CTAB. From speciation diagram in [18], Zn^{2+} ions can interact with NH_4^+ ions and form a $[Zn(NH_3)_4]^{2+}$ complex at a pH value of 8.8. After that ZnO nuclei can form via dehydration reaction and the ZnO can grow preferentially along the *c*-axis or <0001> direction because of its rapid growth rate as mentioned previously.

$$(CH_2)_6N_4 + 6H_2O \longrightarrow 4NH_3 + 6HCHO$$

$$NH_3 + H_2O \leftrightarrow NH_4^+ + OH^-$$

$$Zn^{2+} + 4NH_3 \leftrightarrow [Zn(NH_3)_4]^{2+}$$

$$[Zn(NH_3)_4]^{2+} + 2OH^- \longrightarrow ZnO + 4NH_3 + H_2O$$

Under these experiments, a pH value of final solution (8.8) is lower than the PZC of ZnO, so the surface of ZnO nuclei is surrounded by positively-charged species. When the CTAB was added into the solution, both CTAB and ZnO crystal surface were positively charged at this pH. Therefore, the electrostatic interaction did not occur [19] but CTAB could promote the growth along the other planes, thus spherical shape can form under this condition.

As NH_4OH solution was used, a rod-like shape occurred in all experiments. A pH value of solutions (10.8) is a bit higher than the PZC of ZnO, thus the surface of

ZnO is surrounded by negatively charged species and therefore the electrostatic interaction can affect the rod-like formation as in the case of NaOH solution. The chemical reactions were followed and proposed based on the speciation diagram in [18].

$NH_3 + H_2O \leftrightarrow NH_4^+ + OH^-$

$Zn^{2+} + 2OH^- \leftrightarrow Zn(OH)_2$

$Zn(OH)_2 + OH^- \leftrightarrow Zn(OH)_3^-$

$Zn(OH)_2 \leftrightarrow ZnO + H_2O$

3.2 Band gap evaluation

In this part, the dependence of optical band gap on particle shape and size was studied. S1, S2 and S3 are representative samples to investigate the effect of crystallite size whereas S3 and S6 are representative samples to study the effects of particle shape.

In this study, the E_g value can be estimated from a linear portion of the $(\alpha E)^2$ versus E curves (Fig 3 (a)) plotted from the following equation [20]:

$$(\alpha E)^2 = E_D(E - E_g) \tag{2}$$

where E is the photon energy, E_g is the optical band gap, E_D is a constant and α is an absorption coefficient that could be approximated by:

$$\alpha = \frac{A}{d} \tag{3}$$

where A is the measured absorbance and d is the thickness of the cell (0.4 cm) and E can be estimated by:

$$E = \frac{1{,}240}{\lambda} \tag{4}$$

where λ is the measured wavelength (nm).

To investigate the effect of crystallite size, S1, S2 and S3 (rod-like structure) were selected so as to omit the shape effect. The estimated E_g value of these samples is presented in Table 2. It is evident that the E_g value decreased when the crystallite size decreased. It has been recognized that the E_g value occurred from an electronic transition between the filled valence bands to the empty conduction bands and ZnO single crystal normally shows the E_g value of about 3.37 eV. Obviously, the E_g value of all samples is smaller than that of the E_g value of a single crystal. This is due to the imperfections or defect formations within a forbidden band of ZnO powders. So, the E_g value obtained from the electronic transition between the filled valence states to the energy level of the generated defects instead of the transition between the valence band to the conduction band as usual. To verify the defect, the room temperature PL spectra were measured in a range of 450-800 nm as presented in Fig. 4 (a). A broad visible emission occurred by envelop spectra of multiple emission bands originating from many defects such as zinc vacancy (V_{Zn}), zinc interstitial (Zn_i), oxygen vacancy ($V_{\dot{O}}$), oxygen interstitial (O_i), antisite oxygen (O_{Zn}), etc. [1]. Based on the spectra obtained, higher emission intensity obtained from a smaller size or higher surface area to volume ratio. In fact, ZnO has many defects on its surface which can adsorb O^{2-} and O^{-} ions to form oxygen vacancies. Therefore, it could be presumed, that the sample with a higher intensity has more defect concentration. In this study, S3 performed the highest emission intensity; it suggests that this sample has the highest defect concentration, so it is reasonable to conclude that this sample shows the smallest E_g value.

To study the influence of particle shape on E_g value, the S3 (rod-like) and S6 (spherical shape) were selected. The E_g value obtained from S6 (spherical shape) is higher than the E_g value obtained from S3 (rod shape). The room temperature PL

spectra of S3 and S6 show slightly different emission intensity in the visible region as shown in Fig. 4(a). Therefore, the defect concentration (E_0) obtained from the reciprocal value of the slopes from the linear part of the curves of ln(α) versus E was determined and the results are given in Table 2. From the results obtained, we can confirm that the E_g value depended upon the defect concentration. So, it could be pointed out that the sample with higher defect concentration gave a smaller E_g value.

Regarding S3, the broad band in the visible region (450-800 nm) was fitted with a Gaussian function as presented in Fig. 4(b). By the fitting result, a green band centered at about 540 nm is attributed to oxygen vacancies as well as yellow band (640 nm) and an infrared band (740 nm) are due to interstitial ions or extrinsic defects [21, 22].

3.3 Photocatalytic activity

The temporal change in MB concentration for ZnO powders with different sizes and shapes are depicted in Fig 5. It is clearly observed that the maximum absorbance of 665 nm decreased as a function of UV irradiation time. This is due to the breaking of the conjugated π-system in the MB chain [23], consequently very pale white solutions were obtained, indicating that the auxochromic groups were degraded. Fig. 6 shows the decolorization efficiency (%) of ZnO powders calculated by the following equation.

$$y(\%) = \frac{C_0 - C}{C_0} x100 \qquad (5)$$

where y is the decolorization efficiency, C_0 is the initial MB concentration and C is the MB concentration after irradiation at a given time.

As can be seen, the decolorization efficiency of all samples increased when the irradiation time was increased and the decolorization efficiency was higher than 90% after irradiating for 90 min. After the suspensions were irradiated by the UV light with energy higher than the band gap, the electrons (e^-) in the valence band can be excited to the empty conduction band and the holes (h^+) occurred suddenly in the valence band. When the photoelectrons were trapped by oxygen that acted as an electronic acceptor and a superoxide radical anion (O_2^-) were generated subsequently whereas the holes were trapped by MB and these holes acted as an electronic donor to oxidize the MB [24].

Considering the decolorization efficiency of S1, S2 and S3 after being irradiated for 90 min, it is evident that the sample with a rod-like shape and larger E_g value showed a great powerful oxidation of MB. This is because S1 has the largest E_g value, the photoinduced electrons can stabilize for a long time in the conduction band before coming back to the valence band or we can conclude that the sample with wider E_g value has an appropriate energy potentials of charge carriers that can conduct the redox potential on the sample surface via the separately photogenerated electrons and holes [25]. For this reason, the decolorization efficiency of S1 is higher than that of S2 and S3.

S3 and S6 are representative samples to investigate the effects of particle shape. It was observed that the decolorization efficiency of S6 (spherical shape) after being irradiated for 90 min is stronger than that of S3 (rod-like shape). This is because S6 has a larger E_g value. Thus the decolorization efficiency is higher as mentioned above.

4. Conclusions

The different morphologies of ZnO powders were synthesized via precipitation method by using NaOH, HMTA and NH_4OH as the precipitating agent. In this study, CTAB concentration was higher than its critical micelle concentration, so it acted as a capping agent instead of a micelle formation. The size of ZnO powders decreased as CTAB concentration was increased because CTAB can encapsulate the ZnO powder powerfully. CTAB concentration strongly affected the shape formation when HMTA solution was used. It is evident that the rod-like was altered to spherical shape when CTAB concentration was increased. A larger E_g value was obtained from the sample containing a lower defect concentration. The photocatalytic degradation test suggested that ZnO powders showed a great powerful activity in dye degradation of over 90% after irradiating with the UV light for 90 min. The decolorization efficiency depended upon the E_g values of the samples. The higher efficiency obtained from the sample with larger E_g value because of the retardation of the electron-hole recombination process.

Acknowledgement

This research is supported by Thailand Research Fund (TRF) under the contract number MRG5280125. The authors would like to be thankful the Center for Innovation in Chemistry (PERCH-CIC), Commission on Higher Education, Ministry of Education and the authors would like to acknowledge Michael Benjamin Lane for proof reading our manuscript.

References

[1] N. Samaele, P. Amornpitoksuk, S. Suwanboon, Effect of pH on the morphology and optical properties of modified ZnO particles by SDS via a precipitation method, Mater. Lett. 64 (2010) 500-502.

[2] A.B. Djurisic, A.M.C. Ng, X.Y. Chen, ZnO nanostructures for optoelectronics: Material properties and device applications, Quantum Electron. 34 (2010) 191-259.

[3] A. Chiappini, C. Armellini, A. Chiasera, M. Ferrari, R. Guider, Y. Yestin, L. Minati, E. Moser, G. Nunzi Conti, S. Pelli, R. Retoux, G.C. Righini, G. Speranza, Preparation and characterization of ZnO particles embedded in organic-inorganic planar waveguide by sol-gel route, J. Non-Cryst. Solids 355 (2009) 1132-1135.

[4] S. Rani, P. Suri, P.K. Shishodia, R.M. Mehra, Synthesis of nanocrystalline ZnO powder via sol-gel route for dye-sensitized solar cells, Sol. Energy Mater. Sol. Cells 92 (2008) 1639-1645.

[5] J.H. Sun, S.Y. Dong, Y.K. Wang, S.P. Sun, Preparation and photocatalytic property of a novel dumbbell-shaped ZnO microcrystal photocatalyst, J. Hazard. Mater. 172 (2009) 1520-1526.

[6] N. Takahashi, K. Kaiya, K. Omichi, T. Nakamura, S. Okamoto, H. Yamamoto, Atmospheric pressure vapor-phase growth of ZnO using a chloride source, J. Cryst. Growth 209 (2000) 822-827.

[7] P. Mishra, R.S. Yadav, A.C. Pandey, Growth mechanism and photoluminescence property of flower-like ZnO nanostructures synthesized by starch-assisted sonochemical method, Ultrason. Sonochem. 17 (2010) 560-565.

[8] S. Suwanboon, structural and optical properties of nanocrystalline ZnO powder from sol-gel method, ScienceAsia. 34 (2008) 31-34.

[9] X. Li, G. He, G. Xiao, H. Liu, M. Wang, Synthesis and morphology control of ZnO nanostructures in microemulsions, J. Colloid Interface Sci. 333 (2009) 465-

473.

[10] K. Thongsuriwong, P. Amornpitoksuk, S. Suwanboon, The effect of aminoalcohols (MEA, DEA and TEA) on morphological control of nanocrystalline ZnO powders and its optical properties, J. Phys. Chem. Solids 71 (2010) 730-734.

[11] Z. Yang, L. Lv, Y. Dai, Z. Xv, D. Qian, Synthesis of ZnO-SnO_2 composite oxides by CTAB-assisted co-precipitation and photocatalytic properties, Appl. Surf. Sci. 256 (2010) 2898-2902.

[12] H. Wang, C. Xie, W. Zhang, S. Cai, Z. Yang, Y. Gui, Comparison of dye degradation efficiency using ZnO powders with various size scales, J. Hazard. Mater. 141 (2007) 645-652.

[13] S. Suwanboon, P. Amornpitoksuk, A. Haidoux, J.C. Tedenac, Structural and optical properties of undoped and aluminium doped zinc oxide nanoparticles via precipitation method at low temperature, J. Alloys Compd. 462 (2008) 335-339.

[14] M. Bicer, I Sisman, Controlled synthesis of copper nano/microstructures using ascorbic acid in aqueous CTAB solution, Powder Technol. 198 (2010) 279-284.

[15] A. Degen, M. Kosec, Effect of pH and impurities on the surface charge of zinc oxide in aqueous solution, J. Eur. Ceram. Soc. 20 (2000) 667-673.

[16] H. Usui, The effect of surfactants on the morphology and optical properties of precipitated wurtzite ZnO, Mater. Lett. 63 (2009) 1459-1492.

[17] M.S. Mohajerani, A. Lak, A. Simchi, Effect of morphology on the solar photocatalytic behavior of ZnO nanostructures, J. Alloys Compd. 485 (2009) 616-620.

[18] M.N.R. Ashfold, R.P. Doherty, N.G. Ndifor-Angwafor, D. Jason Riley, Y. Sun, The kinetics of the hydrothermal growth of ZnO nanostructures, Thin Solid Films 515 (2007) 8679-8686.

[19] Y. Ishikawa, Y. Shimizu, T. Sasaki, N. Koshizaki, Preparation of zinc oxide nanorods using pulsed laser ablation in water media at high temperature, J. Colloid Interface Sci. 300 (2006) 612-615.

[20] S. Suwanboon, P. Amornpitoksuk, P. Bangrak, Synthesis, characterization and optical properties of $Zn_{1-x}Ti_xO$ nanoparticles prepared via a high-energy ball milling technique, Ceram. Int. 37 (2011) 333-340.

[21] Z. Hung, D. Yan, M. Yang, X. Liao, Y. Kang, G. Yin, Y. Yao, B. Hao, Preparation and characterization of the biomineralized zinc oxide particles in spider silk peptides, J. Colloid Interface Sci. 325 (2008) 356-362.

[22] X. Zhao, Z. Chen, Y. Luo, L. Wang, Giant enhanced infrared and orange emissions of ZnO nanoparticles induced by rich oxygen atmosphere, Solid State Commun.147 (2008) 447-451.

[23] W.S. Chiu, P.S. Khiew, M. Cloke, D. Isa, T.K. Tan, S. Radiman, R. Abd-Shukor, M.A. Abd. Hamid, N.M. Huang, H.N. Lim, C.H. Chia, Photocatalytic study of two-dimensional ZnO nanopellets in the decomposition of methylene blue, Chem. Eng. J. 158 (2010) 345-352.

[24] Y. Wang, X. Li, N. Wang, X. Quan, Y. Chen, Controllable synthesis of ZnO nanoflowers and their morphology-dependent photocatalytic activities, Sep. Purif. Technol. 62 (2008) 727-732.

[25] A. Mills, S. Le Hunte, An overview of semiconductor photocatalysis, J. Photochem. Photobiol., A. 108 (1997) 1-35.

Figure captions

Fig. 1 XRD patterns of all ZnO samples

Fig. 2 SEM images of all ZnO samples

Fig. 3 (a) The evolution of band gap from the plots of $(\alpha E)^2$ vs. E and (b) the evolution of defect concentration from the plots of $\ln\alpha$ vs. E for ZnO samples with different sizes (S1, S2 and S3) and different shapes (S3 and S6)

Fig. 4 (a) Room temperature PL spectra of ZnO samples with different sizes (S1 S2 and S3) and different shapes (S3 and S6) and (b) the fitting analysis using a Gaussian function of S3

Fig. 5 Temporal change in the concentration of MB monitored from ZnO samples with different sizes (S1, S2 and S3) and different shapes (S3 and S6)

Fig. 6 The efficiency comparison of photocatalytic activity of ZnO samples with different sizes (S1, S2 and S3) and different shapes (S3 and S6)

Table captions

Table 1 The experimental conditions and the crystallite size of all ZnO samples

Table 2 The effect of particle size and shape on band gap energy and defect concentration

Table 1

precipitating agent	sample code	CTAB (mole)	crystallite size (nm)
NaOH (0.16 mole)	S1	0	46.4 ± 13.3
	S2	0.01	43.5 ± 6.6
	S3	0.02	41.3 ± 7.6
HMTA (0.16 mole)	S4	0	43.8 ± 3.5
	S5	0.01	42.6 ± 5.0
	S6	0.02	41.5 ± 6.2
NH_4OH (0.04 mole)	S7	0	42.2 ± 6.4
	S8	0.01	41.5 ± 6.2
	S9	0.02	39.9 ± 5.6

Table 2

Sample code	crystallite size (nm)	E_g (eV)	E_U (eV)
S1	46.4 ± 13.3	3.23	0.09
S2	43.5 ± 6.6	3.21	0.15
S3	41.3 ± 7.6	3.18	0.18
S6	41.5 ± 6.2	3.20	0.10

Fig. 1

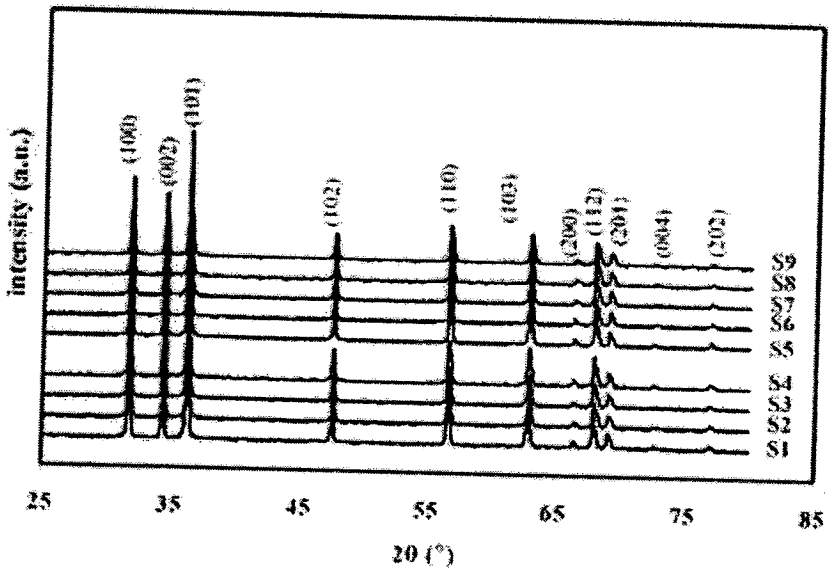

to download high resolution image

Fig. 2

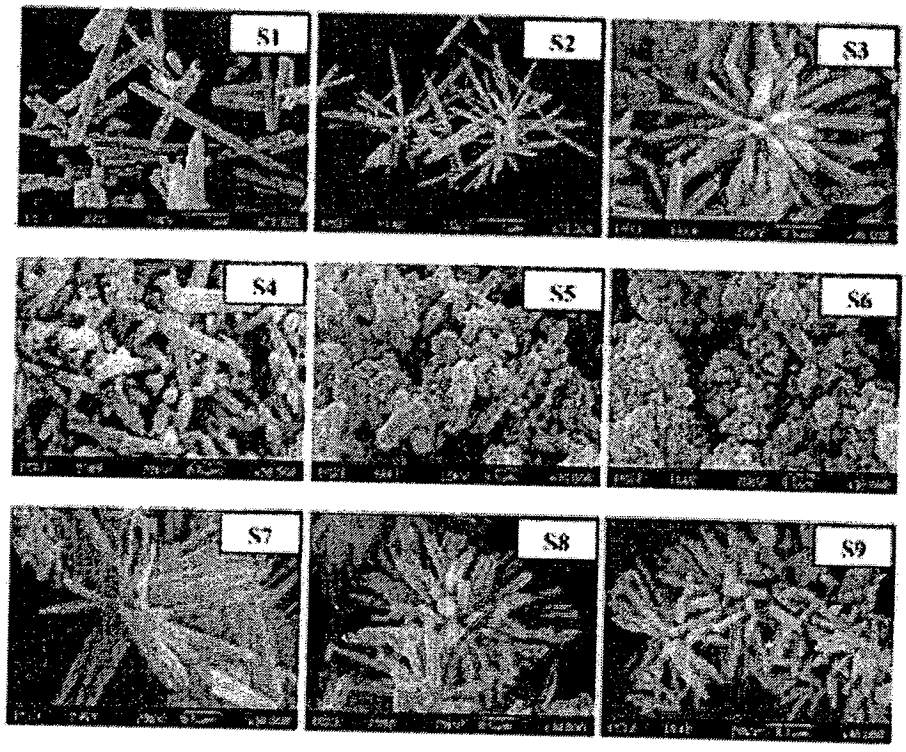

to download high resolution image

Fig. 3

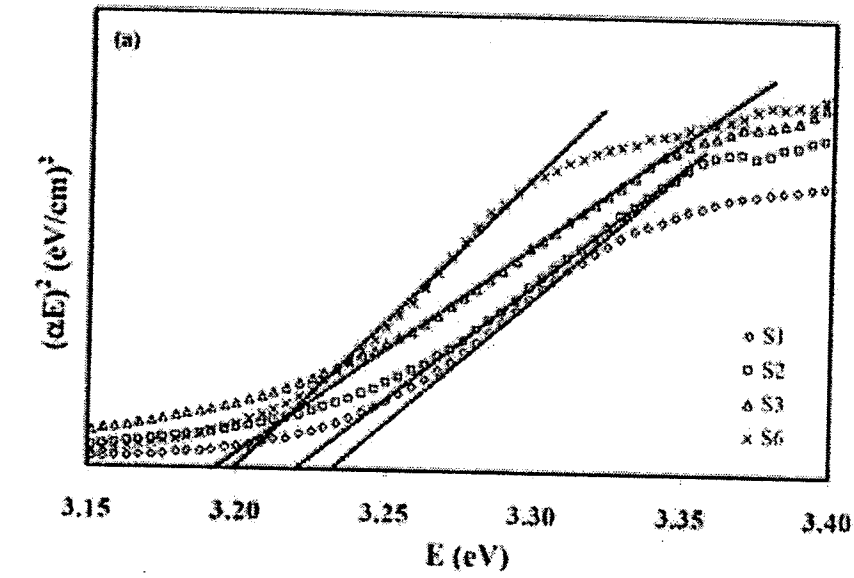

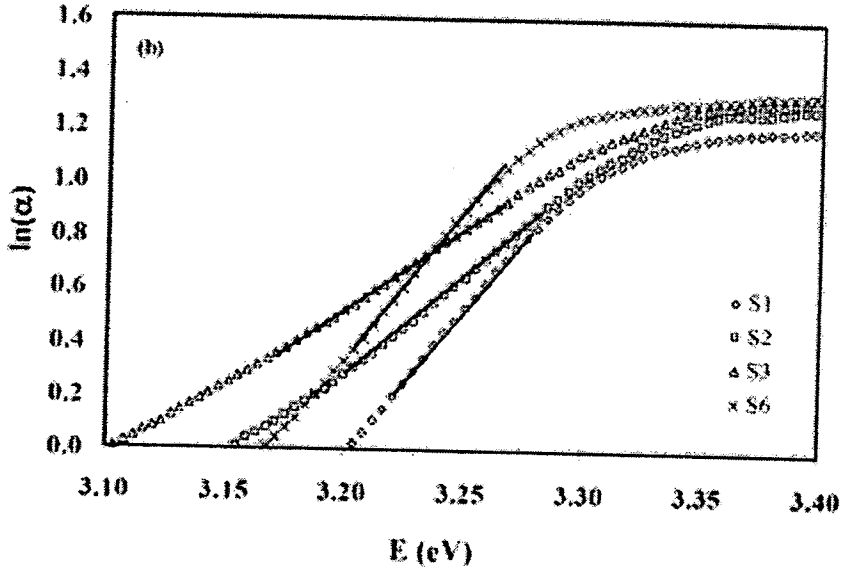

Fig. 4

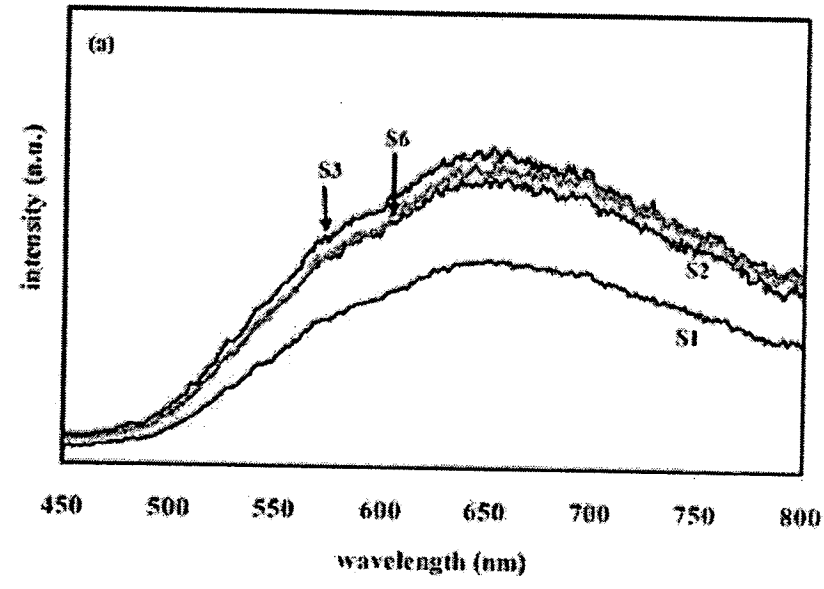

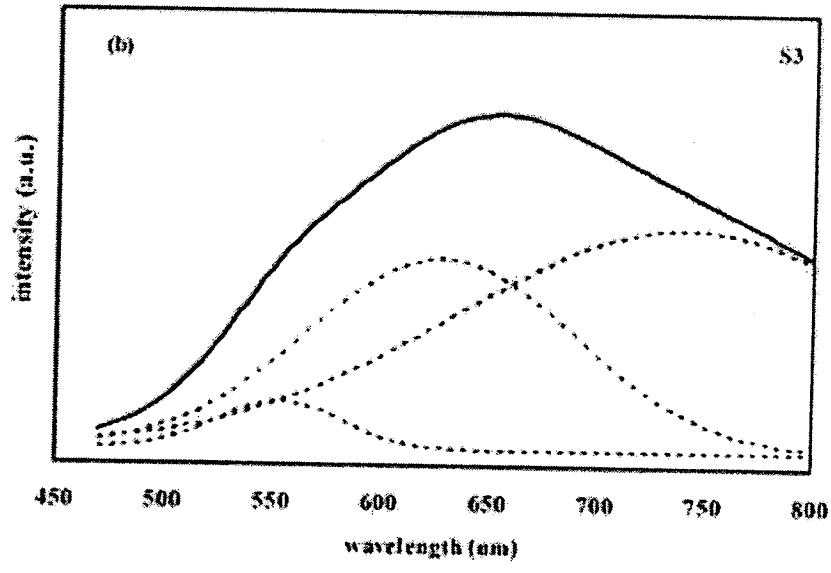

Fig. 5

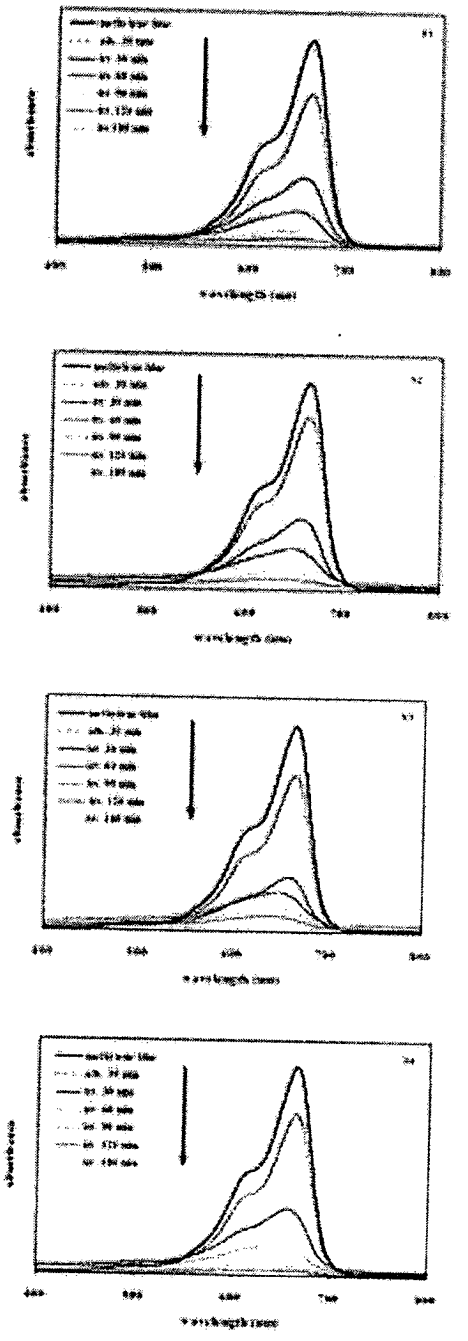

Fig. 6